THE JOURNAL OF BIOLOGICAL CHEMISTRY VOL. 286, NO. 40, pp. 35061–35070, October 7, 2011

Receptor for Advanced Glycation End Products (RAGE) Prevents Endothelial Cell Membrane Resealing and Regulates F-actin Remodeling in a β-Catenin-dependent Manner*

Received for publication, May 15, 2011, and in revised form, August 10, 2011 Published, JBC Papers in Press, August 15, 2011, DOI 10.1074/jbc.M111.261073

Fei Xiong[‡§], Sergey Leonov[¶], Amber Cyan Howard[‖], Shan Xiong[‡], Bin Zhang[‡], Lin Mei[‡], Paul McNeil[‖], Sylvia Simon[¶], and Wen-Cheng Xiong[‡1]

From the [‡]Institute of Molecular Medicine and Genetics and Department of Neurology, Georgia Health Sciences University, Augusta, Georgia 30912, the [¶]Departments of Neuroscience and Translational Sciences, CNS and Pain Innovative Medicines, AstraZeneca R&D Sodertalje, S-15185 Sodertalje, Sweden, the [‖]Department of Cell Biology and Anatomy, Georgia Health Sciences University, Augusta, Georgia 30912, and the [§]School of Medicine, Wuhan University, Wuhan, Hubei 430071, China

Background: RAGE contributes to the vascular pathology associated with multiple disorders, including Alzheimer disease (AD), diabetic complications, and inflammatory conditions. However, the underlying mechanisms remain largely unknown.
Results: RAGE expression in endothelial cells leads to an impaired plasma membrane resealing, altered F-actin remodeling, and increased β-catenin level.
Conclusion: Through β-catenin, RAGE decreases F-actin stress fibers and prevents endothelial membrane repair in response to the injury.
Significance: These results suggest a negative role of RAGE in membrane repair, reveal a new mechanism underlying RAGE regulation of F-actin remodeling, and help our understanding of RAGE involvement in AD and diabetic complication-associated vascular pathology.

Receptor for advanced glycation end products (RAGE), an immunoglobin superfamily cell surface receptor, contributes to the vascular pathology associated with multiple disorders, including Alzheimer disease (AD), diabetic complications, and inflammatory conditions. However, the underlying mechanisms remain largely unclear. Here, using the human umbilical vein endothelial cell line (ECV-304) expressing human RAGE, we report that RAGE expression leads to an altered F-actin organization and impaired membrane resealing. To investigate the underlying mechanisms, we showed that RAGE expression increases β-catenin level, which decreases F-actin stress fibers and attenuates plasma membrane resealing. These results thus suggest a negative function for RAGE in endothelial cell membrane repair and reveal a new mechanism underlying RAGE regulation of F-actin remodeling and membrane resealing.

RAGE[2] is believed to contribute to the vascular pathology associated with AD, diabetic complications, and chronic inflammation (1–5). Full-length RAGE comprises a variable domain and two constant extracellular Ig-like domains, a transmembrane region and a short cytoplasmic tail. The variable domain in particular is believed to be involved in ligand binding (6–8). The link between RAGE and the pathological situations is the multiligand character of the receptor and its ability to sustain cellular activation. Ligands of RAGE include AD-associated amyloid β-peptide (Aβ) (9, 10), diabetes-associated advanced glycation end products (11), the proinflammatory-associated Mac-1/β2 integrin (12), the S100 family (13), and the high mobility group box 1 (HMGB1) (14).

RAGE appears to contribute to several pathogenic features of chronic disorders of AD and diabetic complications. The adverse consequences of RAGE activation in these chronic disorders primarily result from its interaction with AD-associated Aβ and diabetes-associated advanced glycation end products. Excess amounts of Aβ/AGE trigger elevated RAGE expression, as such further enhancing the detrimental effects of RAGE activation. RAGE expression was found increased in AD-affected regions of the brain, such as the hippocampus and superior frontal cortex (10, 15–17). Apart from neurons and microglia, RAGE levels are also increased in cortical amyloid-laden vessels of cerebral amyloid angiopathy patients and in hippocampal microvessels of AD patients (10, 15–17). Moreover, RAGE expression is significantly higher in different organs of patients with diabetic complications (16, 18). These observations support the hypothesis that a gain of function of RAGE can contribute to the pathological progression of both AD and diabetes-associated vascular complications. In terms of vascular pathology, RAGE is believed to be involved in Aβ translocation across the blood-brain barrier (BBB), leading to increased Aβ accumulation and amyloid plaque burden in the brain (15). In addition, RAGE has been reported to be involved in Aβ-mediated migration of monocytes across the BBB endothelial monolayers (19). However, how RAGE regulates endothelial cell membrane permeability, a cellular process crucial for our understanding of vascular pathology associated with AD and/or diabetic complications, remains to be determined.

* This work was supported, in whole or in part, by National Institutes of Health, NIAMS, Grant AR048120 (to W.-C. X.). This study was also supported by AstraZeneca, Inc.
[1] To whom correspondence should be addressed. Tel.: 706-721-5148; Fax: 706-721-8685; E-mail: wxiong@georgiahealth.edu.
[2] The abbreviations used are: RAGE, receptor for advanced glycation end products; AD, Alzheimer disease; Aβ, amyloid β-peptide; BBB, blood-brain barrier; AJ, adherens junction; TJ, tight junction.

Here, using the human umbilical vein endothelial cell line ECV-304, we report that overexpression of human RAGE causes a plasma membrane repair deficit. Further studies demonstrate that RAGE expression leads to an increase of β-catenin that may be due to RAGE inhibition of GSK3β- mediated β-catenin phosphorylation and degradation. Increased β-catenin results in a decrease of F-actin stress fibers and an impairment of membrane resealing. These results suggest an important role for RAGE in remodeling the actin cytoskeleton and in inhibition of the plasma membrane resealing, revealing a potential cellular mechanism underling RAGE involvement in AD and diabetic complication-associated vascular pathology.

EXPERIMENTAL PROCEDURES

Antibodies—RAGE antibodies were purchased from R&D Systems (monoclonal antibody (mAb) 11451 and goat polyclonal antibody 1145) and from Chemicon International (mAb 5328). Rabbit polyclonal anti-RAGE antibodies were also generated using the fusion protein of GST-RAGE-C-terminal tail as the antigen, as described previously (20). Other monoclonal antibodies were purchased from BD Transduction Laboratories (β-catenin, p120^{cas}, α-catenin, VE-cadherin, GSK3β, and GSK3β(pY216)), Upstate Biotechnology, Inc. (Santa Cruz, CA) (β1-integrin), and Sigma (β-actin). Polyclonal antibodies were purchased from Abcam (Occludin), Santa Cruz Biotechnology, Inc. (Syndecan-1), Zymed Laboratories Inc. (ZO-1), and Cell signaling Technology, Inc. (phospho-β-catenin (Ser^{33}/Ser^{37}/Thr^{41}) and phospho-β-catenin (Thr^{41}/Ser^{45})).

Expression Vectors and Generation of Lentiviral Particles—The "mock" vector (pTZ) (from Open Biosystems or AstraZeneca) was used for generation of the human RAGE lentiviral construct. A trans-lentiviral packaging system from Open Biosystems (catalog no. TLP4614 or TLP4615) was used for generation of lentiviral particles according to the manufacturer's protocol.

The plasmids encoding the scramble shRNA and shRNA·β-catenin-1196 were generated as described previously (21). The GFP·β-catenin plasmid was kindly provided by Dr. X. Yu (Chinese Neuroscience Institute, Shanghai, China). The Myr-GFP·β-catenin plasmid was generated by insertion of sequence of myristoylation site 5′-GGT CTG TAC GCG TCT AAA CTG TCT-3′ using the QuikChange II XL mutagenesis kit (Stratagene, La Jolla, CA) as described by the manufacturer. For insertion, the primers used were b-cat-F (5′-CCG GTC GCC ACC ATG GGT CTG TAC GCG TCT AAA CTG TCT GTG AGC AAG GGC GAG-3′) and b-cat-R (5′-CTC GCC CTT GCT CAC AGA CAG TTT AGA CGC GTA CAG ACC CAT GGT GGC GAC CGG-3′). All constructs were verified by complete sequencing of the inserts.

Cell Culture and Transfection—Human endothelial cell line (ECV-304) and human RAGE transduced ECV-304 stable cell lines were provided by AstraZeneca. These cell lines were cultured in M199 medium supplemented with 10% FBS (Invitrogen), 100 IU/ml penicillin, and 100 μg/ml streptomycin (Mediatech, Inc., Herndon, VA). HEK293 cells were maintained in DMEM (Fisher) supplemented with 10% FBS (Invitrogen), 100 IU/ml penicillin, and 100 μg/ml streptomycin (Mediatech, Inc.). For transient transfection, the indicated plasmids were transfected into RAGE-ECV, ECV304, or HEK293 cells by electroporation.

Cell Fractionation Analysis—RAGE and ECV-304 cells were washed twice in ice-cold PBS and mechanically disrupted with scraping in 0.8 ml of homogenization buffer (10 mM HEPES, pH 7.4, 1 mM EDTA, 0.25 M sucrose) plus Complete miniprotease inhibitors (Roche Applied Science) at 4 °C. Cells were further homogenized by 10 strokes of a Dunce homogenizer followed by five passages through a 27-gauge needle. Cell lysates were then centrifuged at 600 × *g* for 10 min at 4 °C. The pellet was resuspended in 0.5 ml of homogenization buffer and centrifuged at 600 × *g* for 10 min at 4 °C, and the resultant pellet was the nuclear fraction. The combined supernatants were centrifuged at 100,000 × *g* for 1 h at 4 °C in an ultracentrifuge (Beckman TL-100) to produce membrane (pellet) and cytosolic (supernatant) fractions.

Co-immunoprecipitation and Western Blot Analysis—For co-immunoprecipitation analysis, cells were lysed in modified radioimmune precipitation buffer (50 mM Tris-HCl, pH 7.4, 150 mM sodium chloride, 1% Nonidet P-40, 0.25% sodium deoxycholate, and proteinase inhibitors). The precleared cell lysates (by incubation and precipitation with 40 μl of protein G agarose (50% of slurry) and 2 μg of normal mouse IgG in the radioimmune precipitation buffer) were incubated with mouse mAb 5328 (2 μg) for 2 h at 4 °C and 50 μl of protein G-agarose in 50% slurry for an additional 12 h at 4 °C. The protein G-precipitated RAGE·β-catenin complex was recovered by brief centrifugation followed by three washes with the radioimmune precipitation buffer. For Western blot analysis, cell lysates or immunoprecipitated protein complexes were resolved by SDS-PAGE and subjected to Western blot analyses with the indicated antibodies as described previously (20, 22).

RT-PCR Analysis—RNA extractions were carried out using TRIzol reagent (Invitrogen). First-strand cDNAs were synthesized by reverse transcription using the SuperScript III First Strand Synthesis kit (Invitrogen). Duplicate quantitative PCRs were carried out using a Qiagen Quantifast™ SYBR® Green PCR kit. The primers for RT-PCR are designed from the β-catenin gene NM_007614. Forward primer was 5′-CCC AGT CCT TCA CGC AAG AG-3′, and the reverse primer was 5′-CAT CTA GCG TCT CAG GGA ACA-3′. All of the experiments were performed according to manufacturer's instructions.

Immunostaining and Confocal Image Analysis—Immunostaining and confocal image analysis were carried out as described previously (41). Briefly, cells were fixed with 4% paraformaldehyde for 20 min at room temperature, permeabilized by 0.1% Triton X-100 for 15 min at room temperature, blocked with 5% bovine serum, and incubated with the indicated antibodies at a dilution of 1:200 to 1:500 for 1 h at room temperature. Double-labeled immunostaining was performed with appropriate fluorescence-conjugated secondary antibodies (Invitrogen) that were incubated at 1:500 dilutions for 1 h at room temperature. Mounting medium with DAPI (Fisher) was used to reveal the nuclei. To examine RAGE cell surface distribution, fixed cells were incubated with blocking serum and the indicated antibodies in the absence of 0.1% Triton X-100. Images were taken by a Carl Zeiss LSM510 META confocal microscope.

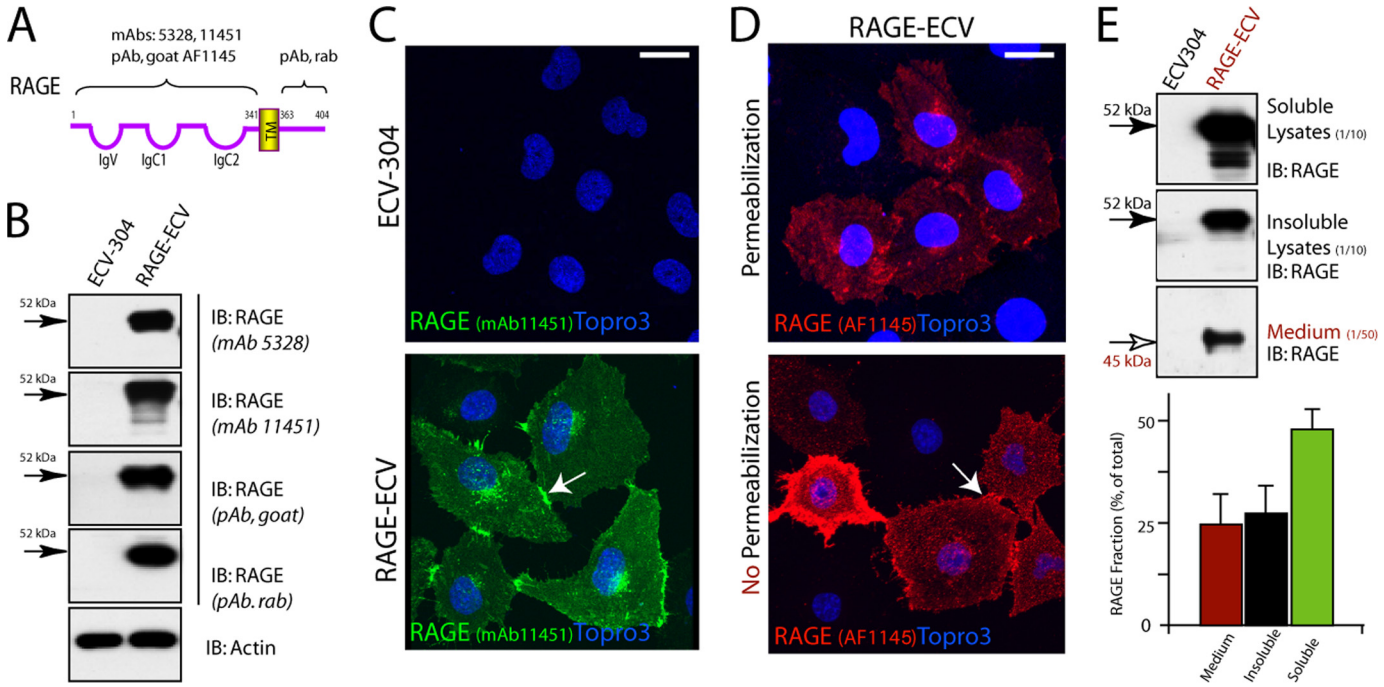

FIGURE 1. **RAGE expression and distribution in ECV-304 and RAGE-ECV cell lines.** *A*, illustration of RAGE structure and the epitope corresponding to each RAGE antibody used. *B*, Western blot analysis of RAGE expression in ECV-304 and RAGE-ECV cell lines. RAGE-ECV cell line was generated by infection of ECV-304 cells with lentivirus encoding human RAGE (amino acids 1–402). Mixed RAGE-expressing cells (with high and lower levels of RAGE) were maintained, and the cell lysates were subjected to Western blot analysis using the indicated RAGE antibodies. *C*, immunostaining analysis of RAGE distribution in ECV-304 and RAGE-ECV cells. Cells plated onto coverslips were immunostained with the monoclonal anti-RAGE (mAb 11451) antibody and analyzed by confocal imaging. *D*, immunostaining analysis of RAGE cell surface distribution in RAGE-ECV cells. Fixed cells were treated with (permeabilization) or without (no permeabilization) 1% Triton X-100 for 20 min at room temperature. Cells were then immunostained with the polyclonal anti-RAGE (goat) antibody (AF1145). In *C* and *D*, the *arrows* indicate the cell junctional distribution of RAGE. *Bars*, 50 μm. *E*, Western blot analysis of RAGE protein in 1% Triton X-100-soluble and -insoluble lysates and in culture medium. The percentage of RAGE in each fraction over total RAGE protein was quantified and illustrated in the *bottom panel*. *Error bars*, S.D.

A Laser-based Plasma Membrane Resealing Assay—A single cell laser assay was used for measuring cell membrane repairing activity as described previously (23). In brief, RAGE-ECV, ECV304, or ECV304 cells expressing the indicated plasmids were plated, respectively, onto a glass-bottom culture dish filled with PBS solution containing 1.26 mM Ca^{2+} and 0.82 mM Mg^{2+}. Individual cells were selected for the assay. Membrane damage was induced in the presence of 2.5 μM FM 1-43/FM4-64 dye (Molecular Probes) with a two-photon confocal laser-scanning microscope (LSM 510, Zeiss) coupled to a 10-watt argon/titanium sapphire laser (Spectra-Physics Lasers Inc.). After images were scanned predamage, a 12 × 12-μm area of the membrane on the surface of the cell periphery was irradiated at 80% power for 1.00 s. Fluorescence images were captured at 5-s intervals for 5 min after the initial damage. The fluorescence intensities at the damaged site were measured by LSM 510 software and quantified using ImageJ software.

Statistical Analysis—Statistically significant differences between groups *versus* control were obtained with Student's *t* test, and significant differences are indicated by asterisks when $p < 0.05$.

RESULTS

RAGE Localization at Cell Surface and Enriched in Cell-Cell Junctions in the ECV-304 Cell Line Transduced with Human RAGE—The up-regulation of RAGE in both AD and diabetic patients and animals led to the hypothesis that gain of RAGE function may contribute to the pathogenesis of these disorders. We thus generated a stable RAGE expression cell line, RAGE-ECV, in which ECV-304 cells were transduced with lentivirus encoding human RAGE (Fig. 1*A*). RAGE was undetected or very weakly detected in the parental ECV-304 cells (Fig. 1, *B* and *C*). By contrast, high levels of RAGE protein were detected in the RAGE-ECV cell line by both Western blot and immunostaining analyses using RAGE-specific antibodies (Fig. 1, *B* and *C*). RAGE protein appeared to be largely distributed on the cell surface and enriched at the cell-cell junctions (Fig. 1*C*). To further confirm RAGE protein in the cell surface, we performed immunostaining analysis in the absence or presence of 0.1% Triton X-100, which allows antibody to penetrate cell membrane into the cells. RAGE was detected at a high level in the cell surface and appeared to be "aggregated" in the cell-cell junctional sites (Fig. 1*D*). We also compared RAGE protein levels between Triton X-100-soluble and -insoluble lysates (Fig. 1*E*). The majority (~60%) of RAGE protein appeared to be soluble (Fig. 1*E*). In addition, the soluble RAGE in the culture medium was also detected in RAGE-ECV cells (~25%) (Fig. 1*E*), which may be due to RAGE shedding caused by a membrane-associated proteinase, such as ADAM10 (24).

Impaired Membrane Resealing and Altered F-actin Structures in RAGE-ECV Cells—RAGE, a cell surface glycoprotein, led to the speculation that it may play a role in regulating plasma membrane plasticity because of cell surface glycoproteins are implicated in this event (25). To test this hypothesis, a plasma membrane resealing assay was carried out in ECV-304

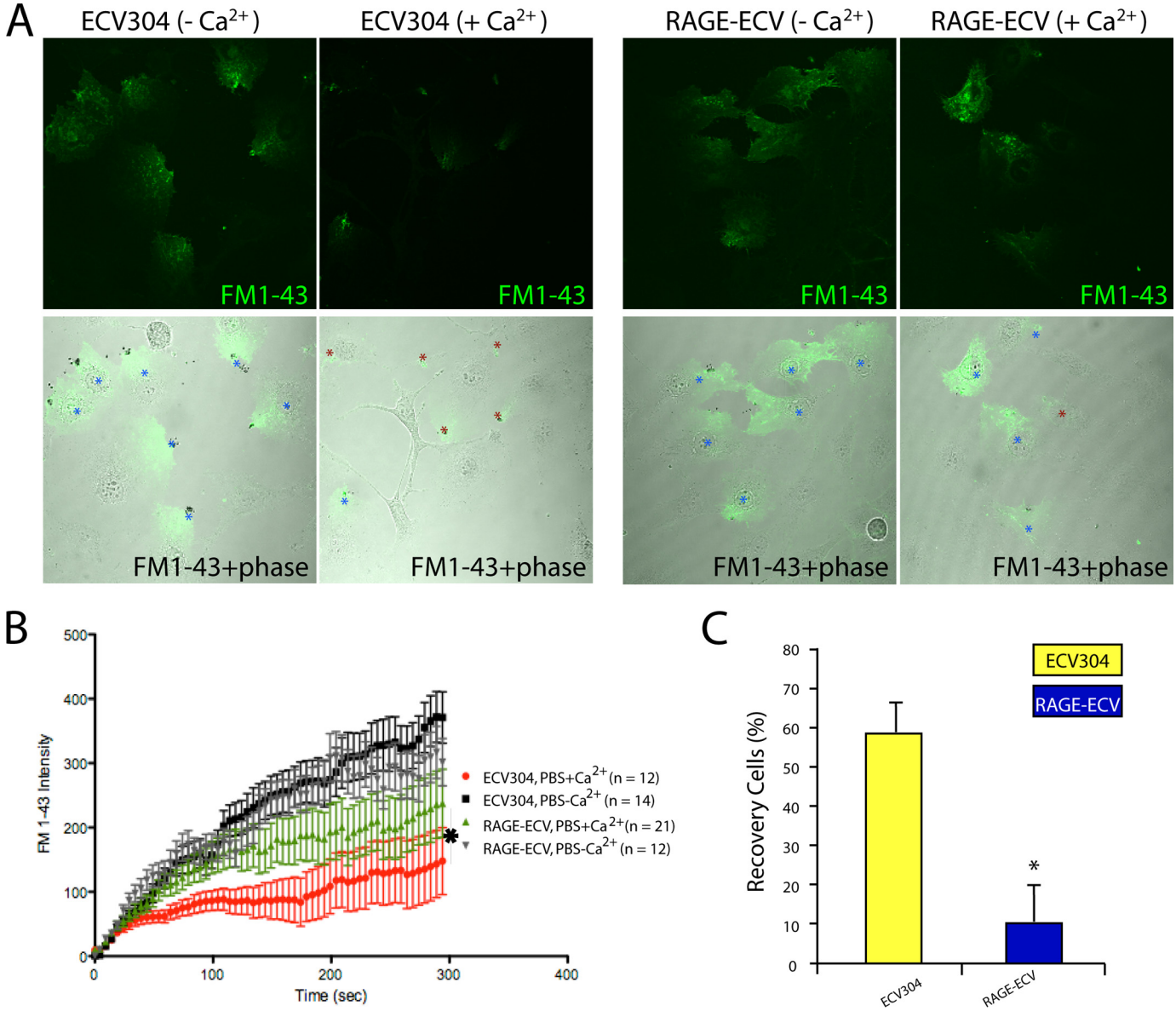

FIGURE 2. **Impaired plasma membrane resealing in RAGE-ECV cells.** *A*, ECV-304 and RAGE-ECV cells were laser-injured in the presence and absence of Ca^{2+}-containing PBS and FM1-43, a cell membrane-impermeable fluorescence dye. Time lapse images were recorded. Images shown were after the injury (300 s). *Stars* indicate injury sites. *B*, quantification of FM1-43 dye uptake. RAGE-ECV cells showed significantly more dye influx (*, $p < 0.05$, significant difference by repeated measures analysis of variance) when compared with ECV-304 cells. *C*, quantification of percentage of cells with resealing response (cells with no significant increase of FM1-43 dye uptake). Shown are means ± S.E. (*error bars*); $n = 12–21$; *, $p < 0.05$, compared with ECV-304 control (*t* test).

and RAGE-ECV cells after laser-induced local membrane injury at the cell periphery. The membrane injury and repair were revealed by a membrane-impermeable fluorescent dye (FM1-43) as it entered the cell through the injured membrane site and disappeared upon membrane resealing. The resealing process depends on various Ca^{2+}-induced mechanisms (26). As shown in Fig. 2, the majority (~60%) of ECV-304 cells showed an efficient membrane resealing response in a Ca^{2+}-dependent manner. Remarkably, this calcium-induced resealing response was attenuated in RAGE-ECV cells (Fig. 2, *A–C*). Only ~10% RAGE-ECV cells showed repair response after the injury (Fig. 2*C*). These results thus suggest a negative effect by RAGE on plasma membrane repair.

Local actin cytoskeletal depolymerization is necessary for membrane resealing events (27). We thus examined if F-actin structures are altered in RAGE-ECV cells. Phalloidin staining analysis of F-actin in ECV-304 and RAGE-ECV cells revealed an increase of filopodia-like structures but a decrease of stress fibers in RAGE-ECV cells as compared with the ECV-304 control cells (Fig. 3, *A* and *B*). Filopodia-like structures were able to interconnect cells (Fig. 3*A*). We then examined if RAGE was associated with these F-actin-positive filopodia-like structures. Indeed, a colocalization of RAGE with F-actin labeled by phalloidin at the filopodia was observed (Fig. 3*A*). These F-actin structures appeared to be dynamic and were regulated by cell density, and the majority (~60%) of RAGE-ECV cells with filopodia-like structure was found at lower cell density culture (data not shown). These results suggest that RAGE expression is sufficient to reorganize F-actin cytoskeleton with an increase of filopodia but a decrease of stress fibers, providing a potential

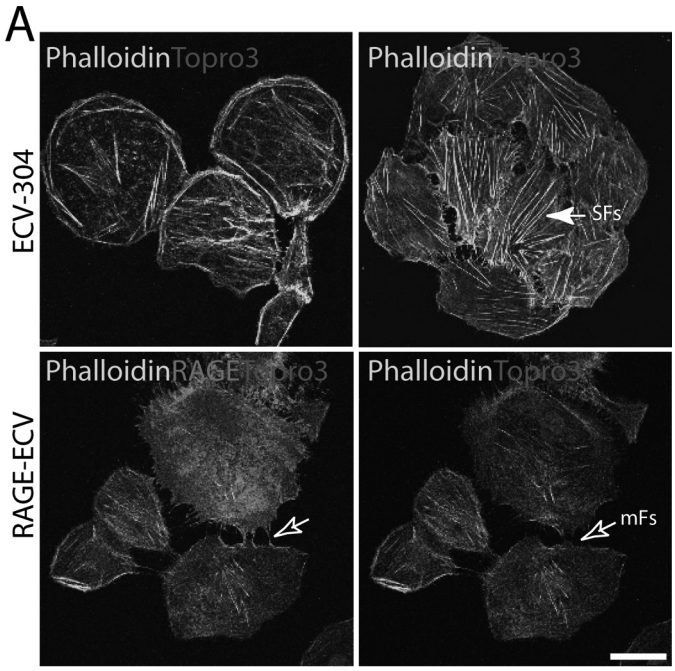

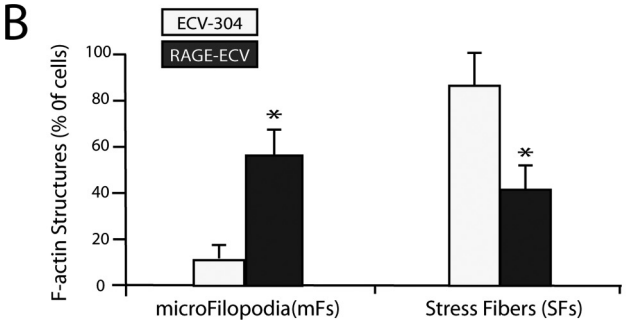

FIGURE 3. **Decrease of stress fibers but increase of microfilopodia in RAGE-ECV cells.** *A*, increase of F-actin-containing microfilopodia (*mFs*) but decrease of stress fibers in RAGE-ECV cells. Cells cultured onto glass coverslips were fixed, permeabilized with Triton X-100, and subjected to immunostaining analysis using phalloidin (to label F-actin) and RAGE (mAb 11451) antibody. The *filled arrow* indicates stress fibers (*SFs*) (which are long F-actin filaments across the cell body). The *open arrows* refer to the microfilopodia (short F-actin filaments at the cell periphery). *Bar*, 50 μm. *B*, quantification analysis of data from *A*. For F-actin structure quantification, each experiment (with duplicate coverslips) was repeated 2–3 times. For each coverslip, ~10 images were taken at different areas, and the percentages of the total number of cells with microfilopodia or stress fibers were calculated and presented. Shown are means ± S.D. (*error bars*), $n > 50$ (number of cells); *, $p < 0.01$, significant difference from the ECV-304 control.

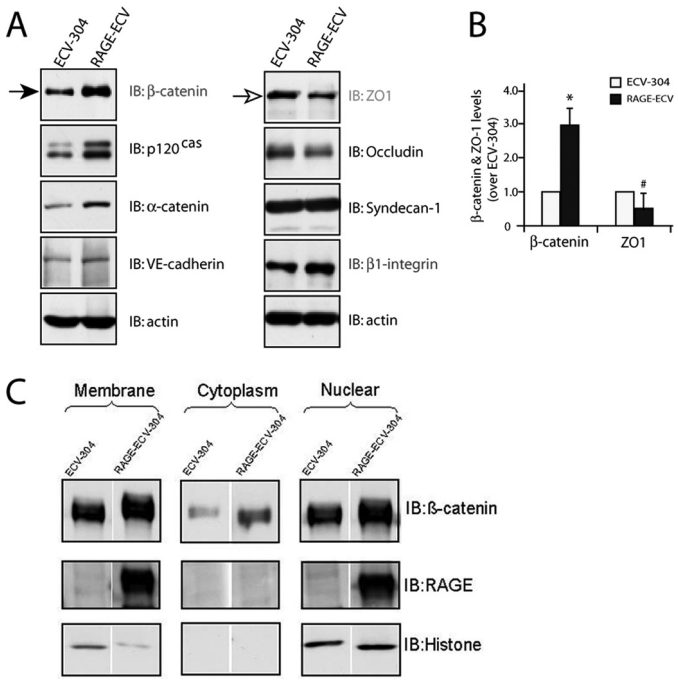

FIGURE 4. **Increase of β-catenin and decrease of ZO-1 in RAGE-ECV cells.** *A*, Western blot analysis of β-catenin, ZO-1, and other indicated proteins in ECV-304 and RAGE-ECV cells. *B*, quantification analysis of β-catenin and ZO-1 levels in *A*. Shown are means ± S.D. (*error bars*); $n = 3$; *, $p < 0.01$, significant difference from the ECV-304 control (*t* test). *C*, Western blot analysis of β-catenin in membrane, cytosol, and nuclear fractions of cell lysates from ECV-304 and RAGE-ECV cells. In *A–C*, lysates, obtained from both ECV-304 and RAGE-ECV cells cultured at lower density (~70% confluence), were subjected to Western blot analysis (*A* and *B*) or fractionation (*C*), as described under "Experimental Procedures." *IB*, immunoblot.

mechanism underlying RAGE inhibition of membrane resealing.

Increase of β-Catenin and Decrease of GSK3β-mediated β-Catenin Phosphorylation in RAGE-ECV Cells—To further investigate molecular mechanisms underlying RAGE regulation of membrane repair and F-actin remodeling, we compared the expression of major cell adhesion-associated proteins in ECV-304 and RAGE-ECV cells. The two major types of cell-cell junctions formed between endothelial cells are adherens junctions (AJs) and tight junctions (TJs). TJ proteins include occludins, claudins, and junctional adhesion molecules and their adaptors (*e.g.* ZO-1). AJs contain VE-cadherin and its associated catenins (α, β, and p120^{cas}). Interestingly, Western blot analysis demonstrated an increase of β-catenin in RAGE-ECV cells compared with ECV-304 cells (Fig. 4, *A* and *B*). Other AJ-associated proteins, such as α-catenin, p120^{cas}, and VE-cadherin, were also slightly increased in RAGE-ECV cells (Fig. 4*A*). In contrast, ZO-1, a TJ marker, was reduced in RAGE-ECV cells (Fig. 4, *A* and *B*). Focal adhesion kinase, claudin-5, syndecan-1, and β-actin were unchanged (Fig. 4*A*) (data not shown). These results suggest an increase of AJ-associated cell-cell adhesion proteins, especially β-catenin, in RAGE-ECV cells.

Two major pools of β-catenin are present in cells: the AJ junctional (cell membrane) pool and the cytosolic-nuclear pool (28). The cytosolic pool of β-catenin is at low levels normally because it is constitutively phosphorylated by GSK3 and rapidly degraded through the ubiquitin-proteasome system (28). We thus asked which pool(s) of β-catenin is increased in RAGE-ECV cells. Cell fractionation and Western blot analysis indicated that cell membrane, cytosol, and nuclear pools of β-catenin were all higher in RAGE-ECV cells as compared with ECV-304 cells (Fig. 4*C*). These results thus demonstrated that β-catenin in RAGE-ECV cells was increased not only in the cytoplasm and nuclear compartments but also in the cell-cell junctions.

To understand how RAGE increases β-catenin, we first compared the β-catenin transcript level between ECV-304 and RAGE-ECV cell lines by real-time PCR analysis. No significant difference of β-catenin expression was observed (Fig. 5*A*), suggesting that RAGE up-regulation of β-catenin is largely at the post-transcriptional level. We then assessed if β-catenin Ser/

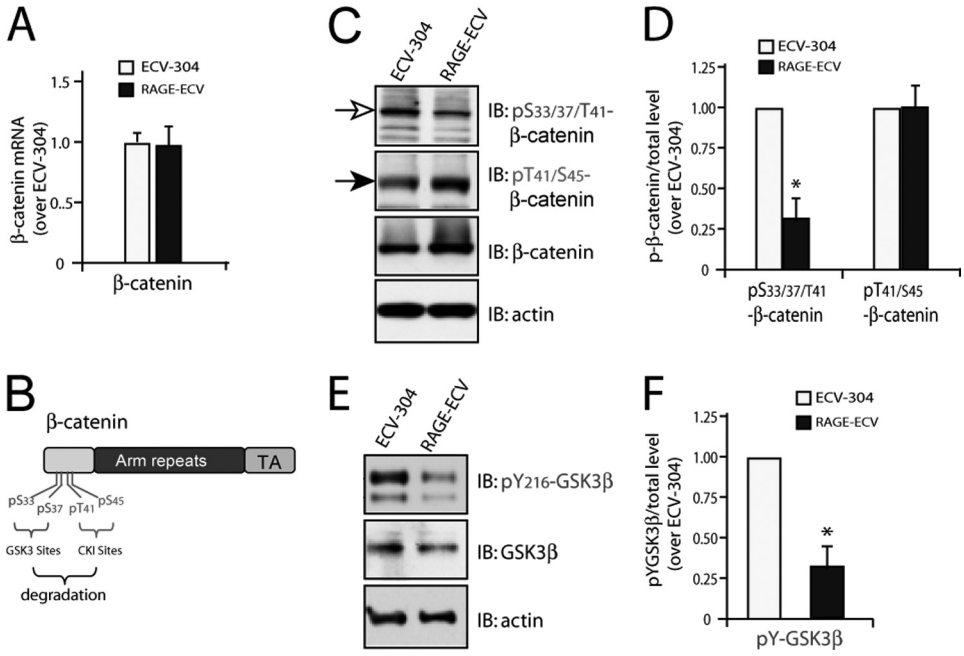

FIGURE 5. **Decrease of GSK3β-mediated β-catenin phosphorylation in RAGE-ECV cells.** *A*, real-time PCR analysis of β-catenin transcript level in ECV-304 and RAGE-ECV cells. RNAs, isolated from indicated cells, were used for the synthesis of cDNAs and real-time PCR analysis. Data were normalized by internal control of GAPDH and presented as -fold over the ECV-304 control (mean ± S.D. (*error bars*), $n = 3$). *B*, illustration of β-catenin phosphorylation sites that induce its degradation. *C*, Western blot analysis of β-catenin phosphorylation using the indicated antibodies. *D*, quantification analysis of the relative β-catenin phosphorylation level. Means ± S.D. ($n = 3$) are presented. *, $p < 0.01$, significant difference from the ECV-304 control. *E*, Western blot analysis of GSK3β tyrosine 216 phosphorylation using the indicated antibodies. *F*, quantification analysis of the relative GSK3β tyrosine phosphorylation level. Means ± S.D. ($n = 3$) are presented. *, $p < 0.01$, significant difference from the ECV-304 control. *IB*, immunoblot.

Thr phosphorylation, an event crucial for β-catenin protein turnover, is altered in RAGE-ECV cells. Threonine 41 and serine 45 in β-catenin are known to be phosphorylated by casein kinase I, which primes β-catenin for subsequent GSK3 phosphorylation at serine 33/37 in the N terminus of β-catenin (Fig. 5*B*) (28, 29). Phosphorylated β-catenin is then recognized by β-Trcp and rapidly degraded by the proteasome (28, 29). Western blot analysis using these phosphorylation state-specific antibodies showed that p33/37/41·β-catenin, but not p41/45·β-catenin, was lower in RAGE-ECV cells *versus* ECV-304 cells (Fig. 5, *C* and *D*), indicating that GSK3, but not casein kinase I, activity may be suppressed by RAGE expression. This notion was further confirmed by Western blot analysis using an antibody specific for tyrosine 216-phosphorylated GSK3β, an active form of GSK3β. Reduced $Tyr(P)^{216}$-GSK3β was observed in RAGE-ECV cells relative to ECV-304 cells (Fig. 5, *E* and *F*). These results thus suggest that RAGE suppression of GSK3β-induced β-catenin phosphorylation may be one of the underlying mechanisms for RAGE increase of β-catenin level.

RAGE Interaction with β-Catenin at Cell-Cell Adhesions—Because RAGE was enriched in cell-cell junctions, where β-catenin is largely localized (Fig. 1*C*), we wanted to examine if RAGE is associated with β-catenin at the AJ junctions, leading to the increase of β-catenin at these structures. Co-immunostaining analysis indeed demonstrated a co-localization of RAGE with β-catenin in RAGE-ECV cells (Fig. 6, *A* and *B*). Again, many filopodia-like structures were present at cell-cell junctions of RAGE-ECV but not ECV-304 cells (Fig. 6, *A* and *B*). These filopodia-like structures were positively labeled not only by RAGE antibody and phalloidin but also by β-catenin antibody (Fig. 6, *A* and *B*). ZO-1 was not detected in these filopodia-like filaments (data not shown). These results suggest that expression of RAGE in ECV-304 cells may cause an increase of an "immature" type of AJs and imply that RAGE may interact with β-catenin. The possible interaction of RAGE with β-catenin was further examined by co-immunoprecipitation analysis of lysates from HEK293 cells expressing RAGE and Myr-GFP·β-catenin. Although we did not detect endogenous β-catenin in the RAGE immunocomplexes (Fig. 6*C*; indicated by *open arrows*), a membrane-associated β-catenin (*e.g.* Myr-GFP·β-catenin) was associated with RAGE immunocomplexes (Fig. 6*C*; indicated by *closed arrows*). These results thus suggest that RAGE may interact with membrane-associated β-catenin.

β-Catenin Mediating RAGE Inhibition of F-actin Stress Fibers and Suppressing Membrane Resealing—We next asked if β-catenin in RAGE-ECV cells contributes to the RAGE-induced decrease of F-actin stress fibers. To this end, a plasmid encoding shRNA-β-catenin (indicated by GFP) was generated, which specifically suppressed β-catenin but not RAGE expression when transfected into RAGE-ECV cells (Fig. 7*A*). Suppressing β-catenin expression in RAGE-ECV cells (indicated by GFP) showed an increase of stress fibers as compared with that of RAGE-ECV cells without GFP expression (Fig. 7*A*), indicating a rescue of this phenotype. Expression of scramble shRNA, on the other hand, had no effect, showing a similar decrease of stress fibers as that in untransfected RAGE-ECV cells (Fig. 7*B*). These results thus demonstrate that up-regulation of β-catenin in RAGE-ECV cells is necessary for the decrease of actin stress fibers by RAGE.

To further test this view, we determined if overexpression of β-catenin in an ECV-304 cell affects F-actin stress fiber formation as RAGE does. Indeed, ECV-304 cells expressing GFP·β-

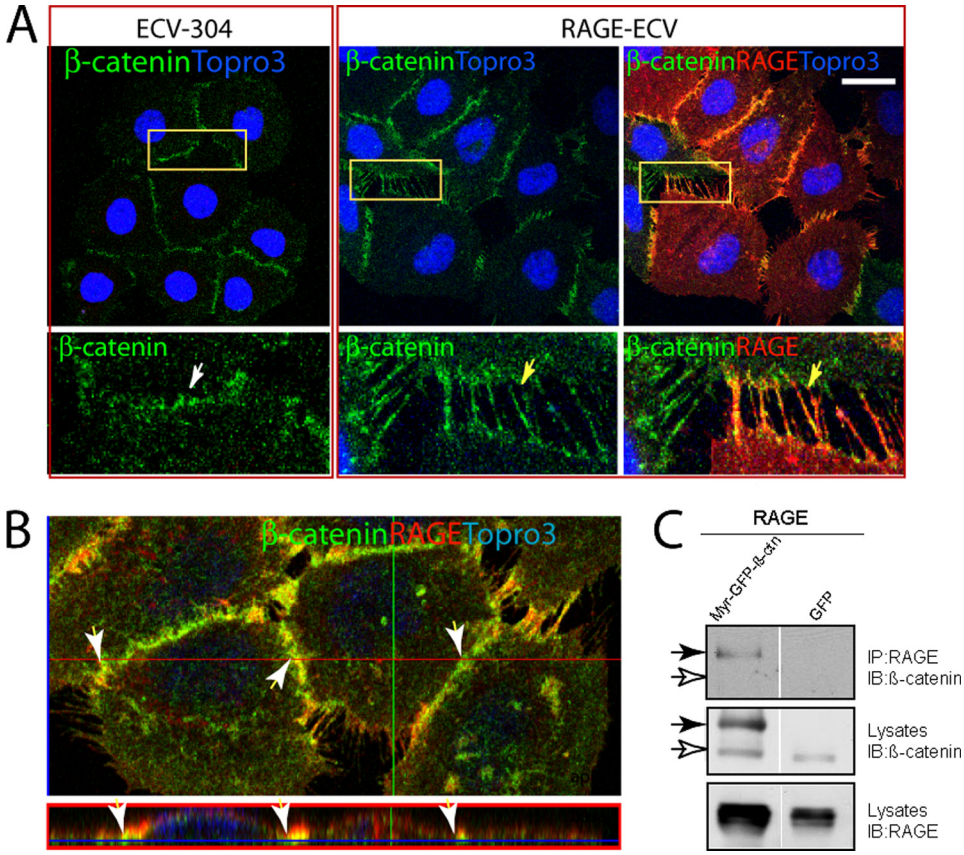

FIGURE 6. **RAGE interaction with β-catenin and alterations of AJs in RAGE-ECV cells.** *A*, co-immunostaining and confocal imaging analyses of RAGE and β-catenin in ECV-304 and RAGE-ECV cells. Cells grown onto glass coverslips were fixed and co-immunostained with the indicated antibodies. Images indicated in the *rectangles* are amplified and shown in the *bottom*. *B*, *x*- and *z*-sections of the confocal images. The *z*-section view (at the *red line* position) is shown at the *bottom*. In *A* and *B*, the *arrows* indicate the junctional staining. *Bars*, 50 μm. *C*, co-immunoprecipitation analysis of RAGE with β-catenin. HEK293 cells were transfected with the indicated plasmids. Cell lysates were subjected to immunoprecipitation (*IP*) using an anti-RAGE antibody (mAb 5328). The resulting immunocomplexes were immunoblotted (*IB*) with the indicated antibodies. The *filled arrows* indicate Myr-GFP·β-catenin, and the *open arrows* indicate endogenous β-catenin.

catenin or Myr-GFP·β-catenin exhibited significant reduction of stress fibers (Fig. 7, *C* and *D*), indicating that β-catenin is sufficient to attenuate stress fiber formation in ECV-304 cells. Taken together, these results suggest that the increase of β-catenin in RAGE-ECV cells is responsible for RAGE inhibition of F-actin stress fibers.

We then asked if β-catenin is also involved in RAGE inhibition of membrane resealing. As shown in Fig. 8, ECV-304 cells expressing GFP showed normal calcium-induced membrane-repairing activity in response to the laser injury. However, cells expressing GFP·β-catenin or Myr-GFP·β-catenin abolished the membrane-resealing effect, exhibiting continued entry of the membrane-impermeable dye (FM4-64) into the injury cells (Fig. 8, *C* and *D*). These results thus suggest that up-regulation of β-catenin in ECV-304 cells also cause an impaired membrane resealing, in a similar manner as that of RAGE, supporting the view for RAGE·β-catenin signaling in inhibition of membrane resealing.

DISCUSSION

Our results using human umbilical vein endothelial cells (ECV-304) overexpressing RAGE demonstrate that RAGE up-regulation (i) increases the β-catenin level, (ii) induces remodeling of the F-actin cytoskeleton with a decrease of stress fibers but an increase of filopodia, and (iii) attenuates plasma membrane resealing. These results led to the speculation that RAGE, via inhibition of GSK3β activity and interaction with β-catenin at cell-cell junctions, increases β-catenin, which inhibits F-actin stress fiber formation and contributes to the impaired membrane resealing.

Plasma membrane injury is common in many cells that operate under conditions of mechanical stress, including skeletal and cardiac muscle myocytes, epithelial cells lining the gastrointestinal tract, and endothelial cells of blood vessels (30). Under normal conditions, plasma membrane can be resealed via various Ca^{2+}-dependent mechanisms. The damaged plasma membrane can be patched with internal membranes delivered to the cell surface by exocytosis, repaired by endocytosis of the injured membrane sites, and/or removed by shedding membrane microparticles (31). Proteins featured in membrane resealing are Ca^{2+} sensors, or their activity is regulated by Ca^{2+} sensors, including families of annexins, synaptotagmins, SNAREs, ferlins, and MG53, a member of the TRIM protein family (32–36). In addition, cell surface glycoproteins are implicated in membrane resealing because lectin binding of cell surface glycoproteins prevents membrane resealing (25). When membrane resealing is impaired, cells undergo death, which

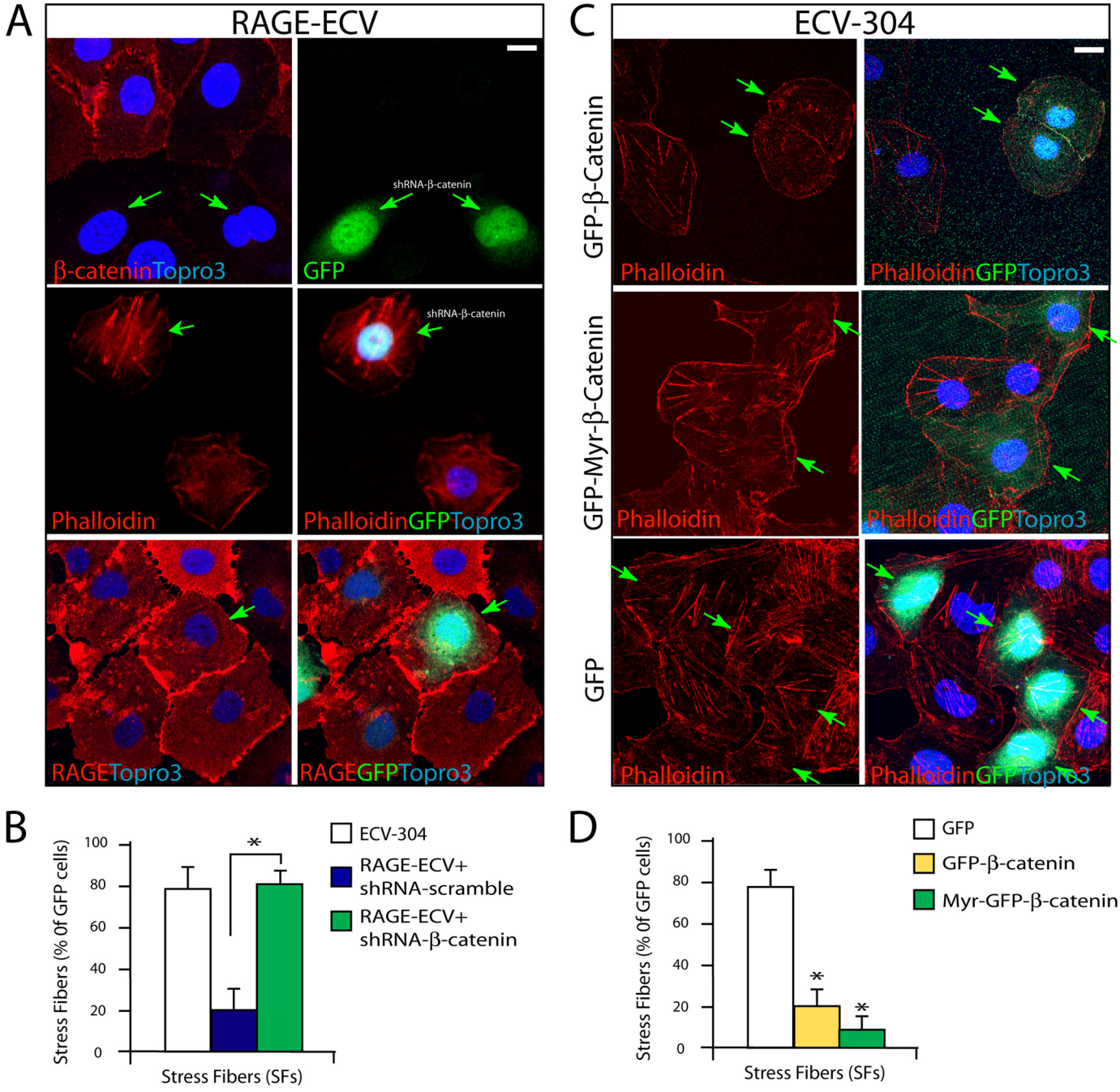

FIGURE 7. **Involvement of β-catenin in RAGE inhibition of F-actin stress fibers.** *A*, RAGE-ECV cells were transiently transfected with shRNA-β-catenin (indicated by GFP) or control scramble shRNA. 48 h after transfection, cells were fixed and subjected to staining analysis using anti-RAGE antibody or phalloidin. *B*, data were quantified and shown as means ± S.D. (*error bars*) ($n = 20$ cells). *, $p < 0.01$, significant difference from the scramble shRNA-expressing cells. *C*, ECV-304 cells were transiently transfected with GFP·β-catenin, Myr-GFP·β-catenin, or GFP control. 48 h after transfection, cells were fixed and subjected to F-actin analysis using phalloidin. *D*, the GFP-positive cells with stress fibers over total GFP-positive cells were calculated, presented as a percentage, and shown as means ± S.D. ($n = 15$). A cell is defined as stress fiber-containing if it contains more than five stress fibers, which are the long F-actin filaments across the cell body. *, $p < 0.01$, significant difference from the GFP-expressing cells. In *A* and *C*, the *arrows* refer to the GFP-positive cells. *Scale bars*, 20 μm.

contributes to the pathogenesis of multiple disorders, including muscular dystrophy (30). RAGE has been implicated in the pathogenesis of AD and diabetes-associated complications(37). Our results using ECV-304 cells, an *in vitro* model for the blood-brain barrier (BBB) (38, 39), suggest a negative role of RAGE in the endothelial cell membrane resealing. Because RAGE is up-regulated under pathological conditions (*e.g.* in AD and diabetic complications), we speculate that increased RAGE at the BBB may lead to an impaired membrane resealing, thereby causing endothelial cell death and promoting further BBB leakage and vascular angiopathy.

How does RAGE attenuate calcium-induced cell membrane resealing? One hypothesis is that RAGE may promote cell surface glycoprotein aggregation, in a manner similar to lectin inhibition of membrane repair (25). Another hypothesis is that RAGE may form homodimers or oligomers by itself, and such complexes alter plasma membrane plasticity. Both hypotheses do not mutually exclude each other and remain to be investi-

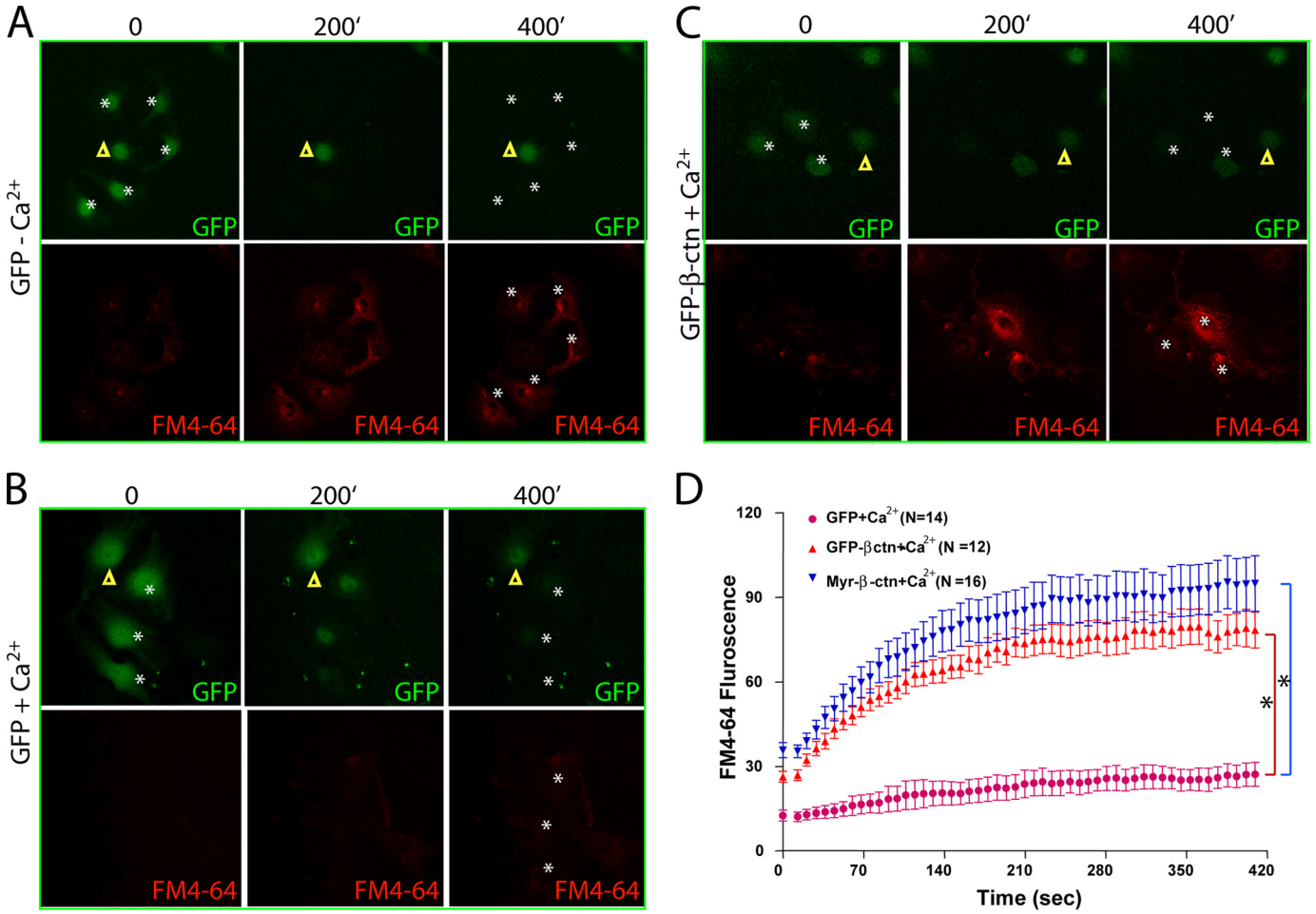

FIGURE 8. ***β*-Catenin inhibition of plasma membrane resealing.** ECV304 cells expressing GFP (*A–B*) or GFP-*β*-catenin (*GFP-β-ctn*) (*C*) were laser-injured in the absence (*A*) and presence (*B* and *C*) of Ca^{2+}-containing PBS and FM4-64, a cell membrane-impermeable fluorescence dye. Time lapse images were recorded. Images shown were before (0 min) and after the injury (200 and 400 min). *Stars*, injury sites; *triangles*, uninjured control cells. *D*, quantification of FM4-64 dye uptake. ECV304 cells expressing *β*-catenin showed significantly more dye influx. *, $p < 0.05$, significant difference by repeated measures analysis of variance, compared with GFP-expressing ECV304 cells. *Error bars*, S.D.

gated further. In addition, our results suggest that RAGE cell surface complex appears to increase *β*-catenin at cell-cell junctions, which may attenuate cell matrix-induced F-actin stress fiber formation and prevent cell membrane resealing. The latter view is in line with the following observations. RAGE-ECV cells exhibit a decrease of stress fibers and focal adhesions (data not shown) but an increase of microfilopodia, implicating a defective ECM-integrin signaling in these cells. The remodeled F-actin structures in RAGE-ECV cells correlate well with the alterations of cell-cell adhesions (*e.g.* increase of immature AJs) and increase of *β*-catenin (Figs. 3–6). Suppression of *β*-catenin expression in RAGE-ECV cells rescued RAGE inhibition of stress fiber phenotype, and overexpression of *β*-catenin in ECV-304 cells decreases their stress fiber formation (Fig. 7). Finally, both increase of *β*-catenin and inhibition of F-actin remodeling are involved in suppressing plasma membrane resealing (Fig. 8) (27). In addition to *β*-catenin, we are aware that RAGE interacts with diaphanous-1, a formin-like protein that is involved in actin cytoskeleton remodeling (40), and RAGE regulation of Rho family GTPases (41), which may be another mechanism(s) underlying RAGE regulation of F-actin remodeling. The exact molecular mechanisms by which RAGE increases *β*-catenin level remain elusive. RT-PCR analysis failed to show an increase of *β*-catenin transcript in RAGE-ECV cells, excluding a transcriptional mechanism. Our results suggest that RAGE may stabilize *β*-catenin protein at the cell-cell junctions, thus preventing its degradation. In support of this view are the observations that cell-cell junctional *β*-catenin is increased in RAGE-ECV cells and that tyrosine 216-phosphorylated GSK3*β* (an active form of GSK3*β*) and GSK3*β* induced serine 33/37 phosphorylation of *β*-catenin (an event causing *β*-catenin degradation) are reduced in RAGE-ECV cells (Figs. 4 and 5). We noted a decrease of ZO-1 in RAGE-ECV cells, which may be a consequence of the increase of *β*-catenin because both AJ and TJ proteins frequently regulate each other. In fact, ZO-1 binds to both tight junction protein, claudin, and adherens junction protein, *α*-catenin (42). On the other hand, the reduced ZO-1 in RAGE-ECV cells may contribute to the increase of immature AJ formation because ZO-1 is required for the formation of beltlike mature AJs in epithelial cells (43).

Taken together, RAGE expression in endothelial cells leads to altered F-actin cytoskeleton and cell-cell adhesions and impaired plasma membrane repair, which may underlie its det-

rimental role in the BBB pathology associated with AD and/or diabetes.

Acknowledgments—We thank Drs. Kristian Sandberg, Patrik Wollberg, and David Malinowsky for generation of the different ECV-304 cell lines.

REFERENCES

1. Miyata, T., Hori, O., Zhang, J., Yan, S. D., Ferran, L., Iida, Y., and Schmidt, A. M. (1996) *J. Clin. Invest.* **98,** 1088–1094
2. Bucciarelli, L. G., Wendt, T., Rong, L., Lalla, E., Hofmann, M. A., Goova, M. T., Taguchi, A., Yan, S. F., Yan, S. D., Stern, D. M., and Schmidt, A. M. (2002) *Cell Mol. Life Sci.* **59,** 1117–1128
3. Schmidt, A. M., Yan, S. D., Yan, S. F., and Stern, D. M. (2001) *J. Clin. Invest.* **108,** 949–955
4. Schmidt, A. M., Hori, O., Cao, R., Yan, S. D., Brett, J., Wautier, J. L., Ogawa, S., Kuwabara, K., Matsumoto, M., and Stern, D. (1996) *Diabetes* **45,** Suppl. 3, S77–S80
5. Yan, S. D., Chen, X., Fu, J., Chen, M., Zhu, H., Roher, A., Slattery, T., Zhao, L., Nagashima, M., Morser, J., Migheli, A., Nawroth, P., Stern, D., and Schmidt, A. M. (1996) *Nature* **382,** 685–691
6. Xie, J., Reverdatto, S., Frolov, A., Hoffmann, R., Burz, D. S., and Shekhtman, A. (2008) *J. Biol. Chem.* **283,** 27255–27269
7. Allmen, E. U., Koch, M., Fritz, G., and Legler, D. F. (2008) *Prostate* **68,** 748–758
8. Ostendorp, T., Leclerc, E., Galichet, A., Koch, M., Demling, N., Weigle, B., Heizmann, C. W., Kroneck, P. M., and Fritz, G. (2007) *EMBO J.* **26,** 3868–3878
9. Yan, S. D., Stern, D., Kane, M. D., Kuo, Y. M., Lampert, H. C., and Roher, A. E. (1998) *Restor. Neurol. Neurosci.* **12,** 167–173
10. Chen, X., Walker, D. G., Schmidt, A. M., Arancio, O., Lue, L. F., and Yan, S. D. (2007) *Curr. Mol. Med.* **7,** 735–742
11. Schmidt, A. M., and Stern, D. M. (2000) *Trends Endocrinol. Metab.* **11,** 368–375
12. Chavakis, T., Bierhaus, A., Al-Fakhri, N., Schneider, D., Witte, S., Linn, T., Nagashima, M., Morser, J., Arnold, B., Preissner, K. T., and Nawroth, P. P. (2003) *J. Exp. Med.* **198,** 1507–1515
13. Hofmann, M. A., Drury, S., Fu, C., Qu, W., Taguchi, A., Lu, Y., Avila, C., Kambham, N., Bierhaus, A., Nawroth, P., Neurath, M. F., Slattery, T., Beach, D., McClary, J., Nagashima, M., Morser, J., Stern, D., and Schmidt, A. M. (1999) *Cell* **97,** 889–901
14. Taguchi, A., Blood, D. C., del Toro, G., Canet, A., Lee, D. C., Qu, W., Tanji, N., Lu, Y., Lalla, E., Fu, C., Hofmann, M. A., Kislinger, T., Ingram, M., Lu, A., Tanaka, H., Hori, O., Ogawa, S., Stern, D. M., and Schmidt, A. M. (2000) *Nature* **405,** 354–360
15. Deane, R., Du Yan, S., Submamaryan, R. K., LaRue, B., Jovanovic, S., Hogg, E., Welch, D., Manness, L., Lin, C., Yu, J., Zhu, H., Ghiso, J., Frangione, B., Stern, A., Schmidt, A. M., Armstrong, D. L., Arnold, B., Liliensiek, B., Nawroth, P., Hofman, F., Kindy, M., Stern, D., and Zlokovic, B. (2003) *Nat. Med.* **9,** 907–913
16. Hong, Z., Yang, Y., Zhang, C., Niu, Y., Li, K., Zhao, X., and Liu, J. J. (2009) *Cell Res.* **19,** 1334–1349
17. Jeynes, B., and Provias, J. (2008) *Curr. Alzheimer Res.* **5,** 432–437
18. Bierhaus, A., Schiekofer, S., Schwaninger, M., Andrassy, M., Humpert, P. M., Chen, J., Hong, M., Luther, T., Henle, T., Klöting, I., Morcos, M., Hofmann, M., Tritschler, H., Weigle, B., Kasper, M., Smith, M., Perry, G., Schmidt, A. M., Stern, D. M., Häring, H. U., Schleicher, E., and Nawroth, P. P. (2001) *Diabetes* **50,** 2792–2808
19. Giri, R., Shen, Y., Stins, M., Du Yan, S., Schmidt, A. M., Stern, D., Kim, K. S., Zlokovic, B., and Kalra, V. K. (2000) *Am. J. Physiol. Cell Physiol.* **279,** C1772–C1781
20. Zhou, Z., Immel, D., Xi, C. X., Bierhaus, A., Feng, X., Mei, L., Nawroth, P., Stern, D. M., and Xiong, W. C. (2006) *J. Exp. Med.* **203,** 1067–1080
21. Zhang, B., Luo, S., Dong, X. P., Zhang, X., Liu, C., Luo, Z., Xiong, W. C., and Mei, L. (2007) *J. Neurosci.* **27,** 3968–3973
22. Cui, S., Xiong, F., Hong, Y., Jung, J. U., Li, X. S., Liu, J. Z., Yan, R., Mei, L., Feng, X., and Xiong, W. C. (2011) *J. Bone Miner. Res.* **26,** 1084–1098
23. McNeil, P. L., Clarke, M. F., and Miyake, K. (2001) *Curr. Protoc. Cell Biol.* Chapter 12, Unit 12.14
24. Raucci, A., Cugusi, S., Antonelli, A., Barabino, S. M., Monti, L., Bierhaus, A., Reiss, K., Saftig, P., and Bianchi, M. E. (2008) *FASEB J.* **22,** 3716–3727
25. Miyake, K., Tanaka, T., and McNeil, P. L. (2007) *PLoS One* **2,** e687
26. McNeil, P. L., and Steinhardt, R. A. (2003) *Annu. Rev. Cell Dev. Biol.* **19,** 697–731
27. McNeil, P. L. (2002) *J. Cell Sci.* **115,** 873–879
28. Wu, D., and Pan, W. (2010) *Trends Biochem. Sci.* **35,** 161–168
29. Xu, C., Kim, N. G., and Gumbiner, B. M. (2009) *Cell Cycle* **8,** 4032–4039
30. McNeil, P. L., and Kirchhausen, T. (2005) *Nat. Rev. Mol. Cell Biol.* **6,** 499–505
31. Bi, G. Q., Alderton, J. M., and Steinhardt, R. A. (1995) *J. Cell Biol.* **131,** 1747–1758
32. Rao, S. K., Huynh, C., Proux-Gillardeaux, V., Galli, T., and Andrews, N. W. (2004) *J. Biol. Chem.* **279,** 20471–20479
33. Han, R., Bansal, D., Miyake, K., Muniz, V. P., Weiss, R. M., McNeil, P. L., and Campbell, K. P. (2007) *J. Clin. Invest.* **117,** 1805–1813
34. McNeil, A. K., Rescher, U., Gerke, V., and McNeil, P. L. (2006) *J. Biol. Chem.* **281,** 35202–35207
35. Zhu, H., Lin, P., De, G., Choi, K. H., Takeshima, H., Weisleder, N., and Ma, J. (2011) *J. Biol. Chem.* **286,** 12820–12824
36. Weisleder, N., Takeshima, H., and Ma, J. (2009) *Commun. Integr. Biol.* **2,** 225–226
37. Yan, S. D., Bierhaus, A., Nawroth, P. P., and Stern, D. M. (2009) *J. Alzheimers Dis.* **16,** 833–843
38. Kuchler-Bopp, S., Delaunoy, J. P., Artault, J. C., Zaepfel, M., and Dietrich, J. B. (1999) *Neuroreport* **10,** 1347–1353
39. Rho, J. H., Roehrl, M. H., and Wang, J. Y. (2009) *Protein J.* **28,** 148–160
40. Hudson, B. I., Kalea, A. Z., Del Mar Arriero, M., Harja, E., Boulanger, E., D'Agati, V., and Schmidt, A. M. (2008) *J. Biol. Chem.* **283,** 34457–34468
41. Hirose, A., Tanikawa, T., Mori, H., Okada, Y., and Tanaka, Y. (2010) *FEBS Lett.* **584,** 61–66
42. Itoh, M., Nagafuchi, A., Moroi, S., and Tsukita, S. (1997) *J. Cell Biol.* **138,** 181–192
43. Ikenouchi, J., Umeda, K., Tsukita, S., Furuse, M., and Tsukita, S. (2007) *J. Cell Biol.* **176,** 779–786